Geoderma 450 (2024) 117028

Contents lists available at ScienceDirect

Geoderma

journal homepage: www.elsevier.com/locate/geoderma

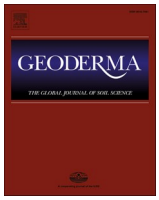

Integrated ground-penetrating radar and electromagnetic induction offer a non-destructive approach to predict soil bulk density in boreal podzolic soil

Sashini Pathirana [a,*], Sébastien Lambot [b], Manokararajah Krishnapillai [a], Mumtaz Cheema [a], Christina Smeaton [a], Lakshman Galagedara [a]

[a] School of Science and the Environment, Memorial University of Newfoundland, Corner Brook, Newfoundland, Canada
[b] Earth and Life Institute, Université catholique de Louvain, 1348 Louvain-la-Neuve, Belgium

ARTICLE INFO

Handling editor: No

Keywords:
Apparent electrical conductivity
Boreal podzolic soil
Dielectric constant
Random forest
Soil compaction

ABSTRACT

Tillage and soil compaction affect soil properties, processes, and state variables influencing soil health, hydrodynamics, and crop growth. Assessing soil compaction levels using traditional methods, such as soil sampling and penetration resistance, is inefficient for scaling up from plot to field scales. Geophysical methods like Ground-penetrating Radar (GPR) and Electromagnetic Induction (EMI) are becoming prominent for assessing soil properties and state variables in agriculture due to their ability to overcome the limitations of traditional methods. However, a research gap exists in non-destructively estimating bulk density changes related to tillage and soil compaction. This study aimed to (1) assess the influence of soil compaction on GPR and EMI responses in boreal podzolic soil and (2) develop and evaluate prediction models to determine soil bulk density using GPR and EMI. The experiment was conducted by compacting loamy sand-textured soil using a lawn roller. GPR data were collected to determine the soil dielectric constant (K_r) and the direct ground wave amplitude (A_{DGW}), along with EMI-measured apparent electrical conductivity (EC_a) under three compaction levels (no, four and ten roller passes). Relationships between K_r, A_{DGW} and EC_a and the average bulk density of 0–0.30 m depth at three compaction levels were tested. A Random Forest (RF) regression approach was employed to identify the most significant variables for predicting bulk density. Simple and multiple linear regression (SLR and MLR, respectively) models were developed using EC_a and K_r and were subsequently evaluated. Results revealed significant differences between the measured bulk density and geophysical data across the tested compaction levels. During the model development, SLR and MLR showed $R^2 > 0.65$, and the model evaluation showed a root mean square error of < 0.14 g/cm^3. This study highlights the potential of using GPR and EMI for the non-destructive prediction of bulk density in the agricultural landscape. However, further research is needed to explore the applicability and limitations of this approach across varying water contents, electrical conductivities, and soil types.

1. Introduction

Soil compaction is a major issue in sustainable agriculture, whether it occurs naturally or results from heavy farming machinery, land use change, and livestock farming (Akinsunmade et al., 2019; Batey, 2009; Hoefer et al., 2010; Hanxiao et al., 2022; Milne & Haynes, 2004; Nawaz et al., 2012). Tillage and soil compaction impact various soil properties, including bulk density, porosity and soil strength, which affect soil processes such as infiltration and drainage (Akinsunmade, 2021; Al-Gaadi, 2012; De Moraes et al., 2017, 2019; Kar et al., 2023; Ren et al., 2022; Nawaz et al., 2012). These altered soil processes subsequently impact state variables, including soil water content (SWC), saturation and soil salinity. Ultimately, changes in soil properties, processes, and state variables adversely affect soil functions by limiting air and water availability, hindering nutrient uptake, and increasing resistance to root growth and mechanical impedance. This leads to increased surface runoff and soil erosion, adversely affecting soil health, crop growth, and yield (Batey & McKenzie, 2006; Liu et al., 2022; Romero-Ruiz et al., 2018; Schmäck et al., 2022; Nawaz et al., 2012).

The traditional methods commonly used to assess soil compaction levels include the measurement of soil bulk density using undisturbed soil sampling (then bulk density) and penetration resistance.

* Corresponding author.
E-mail addresses: epspathirana@mun.ca (S. Pathirana), sebastien.lambot@uclouvain.be (S. Lambot), n62mk@mun.ca (M. Krishnapillai), macheema@mun.ca (M. Cheema), csmeaton@mun.ca (C. Smeaton), lgalagedara@mun.ca (L. Galagedara).

https://doi.org/10.1016/j.geoderma.2024.117028
Received 19 March 2024; Received in revised form 8 September 2024; Accepted 10 September 2024
Available online 16 September 2024
0016-7061/© 2024 The Authors. Published by Elsevier B.V. This is an open access article under the CC BY-NC license (http://creativecommons.org/licenses/by-nc/4.0/).

Determining soil bulk density involves destructive and time-consuming procedures, requiring labor-intensive efforts and only providing point-scale measurements. The accuracy of soil sampling for bulk density determination relies heavily on the operator's expertise, particularly in deep soils, loose soils, and those rich in roots, sand, gravel, and stones (Meng et al., 2023). Similarly, penetration resistance measurements, being resource-intensive and offering point-scale (1D soil profile) data, are susceptible to the influence of both the operator's performance (personal bias) and variations in soil water content (Krzic et al., 2005; Lardy et al., 2022; Ren et al., 2022; Romero-Ruiz et al., 2018). Consequently, accurately estimating soil compaction with high resolution across agricultural landscapes is challenging.

Near-surface electromagnetic geophysical techniques like ground-penetrating radar (GPR) and electromagnetic induction (EMI) offer a non-destructive, efficient and cost-effective means of assessing and comprehending soil properties and state variables in agricultural fields. The majority of previous research has primarily focused on estimating SWC (Badewa et al., 2018; Galagedara et al., 2003a; Galagedara et al., 2003b; Huisman et al., 2003; Klotzsche et al., 2018; Lambot et al., 2004; Mensah et al., 2023; Minet et al., 2010; Pathirana et al., 2024; Wu et al., 2019) and soil salinity (Akramkhanov, 2014; Alsharahi et al., 2016; Corwin & Lesch, 2014; Doolittle et al., 2001; De Carlo et al., 2022; Ferrara et al., 2013; Wijewardana et al., 2017) using GPR and EMI. However, there is a lack of research emphasis on using GPR or EMI for soil bulk density and penetration resistance estimations as indicators of soil compaction (Pathirana et al., 2023).

Recent studies have utilized GPR to assess and map compaction caused by heavy farming machinery in agricultural fields and have identified inverse relationships between GPR wave amplitude and compaction (Akinsunmade, 2021; Akinsunmade et al., 2019, 2021; Wang et al., 2016). Increasing soil bulk density caused greater wave reflection at the soil surface, reducing wave energy transmitted into the ground and penetration depth (Akinsunmade, 2021; Akinsunmade et al., 2019, 2021). Roodposhti et al. (2020) examined how compaction affects the GPR dielectric constant (K_r) and SWC, finding a linear relationship between compaction and K_r when SWC remained constant. Gates et al. (2023) reviewed GPR data processing and analysis methods related to soil horizon thickness and bulk density in forest soils.

With respect to EMI applications, higher apparent electrical conductivity (EC_a) values were reported under compacted conditions, and a linear relationship was found between EC_a and bulk density (Al-Gaadi, 2012; Brevik & Fenton, 2004; Hoefer et al., 2010). Galambošová et al. (2020) observed significantly different EC_a values between compacted and non-compacted areas in silty clay soils, while Ren et al. (2022) revealed a lack of a strong correlation between EC_a and bulk density. However, a positive correlation was observed between EC_a and clay content, thereby suggesting that clay content variability may mask the smaller effects of soil compaction. Schmäck et al. (2022) reported a strong correlation between EC_a and bulk density in the subsoil, but only a weak correlation in the shallow (0–30 cm) plowed layer. By employing machine learning to cluster EMI data, Romero-Ruiz et al. (2024) identified three distinct zones (heavy, moderately, and non-compacted) based on EMI signatures, which aligned well with measured data.

Jonard et al. (2013) explored the effectiveness of GPR and EMI in assessing the impact of different tillage practices on SWC in silty loam soil. The authors highlighted that tillage practices notably affect penetration resistance and SWC in the upper soil layers, and GPR is more sensitive to these changes than EMI. The study confirmed that tillage practices significantly influence GPR measurements but not EMI, underscoring the potential of these techniques for optimizing agricultural management (Jonard et al., 2013).

Theoretical and empirical models, including Archie's law (Archie, 1942) and the Complex Refractive Index Model (CRIM) (Birchak et al., 1974), suggest that soil compaction affects proxies of GPR (K_r) and EMI (EC_a). Archie's law relates EC_a to soil porosity (bulk density). In contrast, CRIM shows that bulk K_r changes with soil porosity and soil water saturation, which is also related to variations in bulk density. Hence, proxies from GPR and EMI can potentially infer soil compaction and bulk density changes.

While the aforementioned studies provide evidence that compaction affects EMI and GPR responses, however limited studies conducted to predict and map soil compaction levels non-destructively in the agricultural landscape. Theoretical models indicate that bulk density correlates with both EC_a and SWC inferred from GPR-measured K_r. Since K_r and EC_a, soil physical properties sensed by GPR and EMI, are influenced by compaction. Therefore, they can serve as proxies for bulk density. GPR wave amplitude is influenced by K_r and EC_a, depending on frequency and reflections (Annan, 2005; Doolittle & Brevik, 2014; Lambot et al., 2006; Wu & Lambot, 2022). Integrating EMI and GPR may enhance bulk density prediction by leveraging the unique strengths of each method. This study introduces a novel approach to non-destructively estimating spatial variability of bulk density by integrating EMI and GPR data at the field scale under different compaction levels. Mapping soil compaction is crucial for precision agricultural management, as deep tillage of compacted layers requires substantial energy, time, and cost. Spatial variability maps of soil compaction could reduce energy needs by targeting tillage efforts on highly compacted areas (Freeland et al., 1998). This integrated approach improves the accuracy of bulk density predictions, thereby enabling better-informed decisions in soil management and agricultural practices.

We hypothesize that predictive models for soil bulk density can be developed using EC_a and K_r proxies from EMI and GPR, respectively, along with direct ground wave amplitude (A_{DGW}) from GPR. Accordingly, the specific objectives were to: (i) assess the impact of soil compaction on GPR (K_r, A_{DGW}) and EMI (EC_a) responses in boreal podzolic soil; and (ii) develop and evaluate the non-destructive predictive capability of prediction models to determine soil bulk density using GPR and EMI.

Fig. 1. The study site located at the Western Agriculture Center and Research Station, Pasadena, Newfoundland, Canada.

Table 1
Basic soil properties of the experimental site show the sandy nature of the soil.

Soil property	Mean value (±Standard deviation)
Sand (%)	87.6 % (±0.94)
Silt (%)	8.9 % (±1.59)
Clay (%)	3.5 % (±1.09)
Soil textural class	Loamy sand
Gravel (% by weight)	31.6 % (±2.04)
Soil organic matter content (% by dry mass basis)	4.77 % (±0.70)

Number of samples $n = 12$.

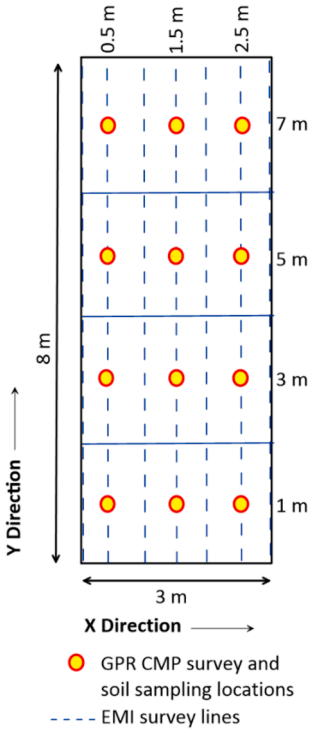

Fig. 2. Field schematic showing the data collection procedure of electromagnetic induction (EMI), ground-penetrating radar (GPR) and soil samples under no passes (NP), four passes (4P) and ten passes (10P).

2. Material and methods

2.1. Study area

The study was conducted in a newly plowed grassland at the Western Agriculture Center and Research Station (49° 04′ 20″ N, 57° 33′ 35″ W), Pasadena, Newfoundland, Canada, which is managed by the Department of Fisheries, Forestry and Agriculture, Government of Newfoundland and Labrador, Canada (Fig. 1). Basic soil properties in the 0 – 0.30 m depth of the studied area are given in Table 1. According to the Canadian soil classification, the loamy sand soil at the studied site is characterized as an orthic humic podzol (Soil Classification Working Group, 1998).

2.2. Experimental compaction

The experimental plots were prepared in the plowed grassland. Initial plowing[1] was done using a moldboard plow and a disk harrow (~0.30 m depth). A day before field data collection, the plots were manually plowed using a spading fork with five tines (0.30 m long). Grasses and rocks were removed manually, and the plots were levelled using a rake.

Fig. 3. Soil compaction (4P and 10P) using a water-filled lawn roller.

In this experiment, a 3 m x 8 m area was selected and divided into four 3 m x 2 m sub-plots (Fig. 2). Field data were collected under three compaction levels: 1) before compaction (labeled as NP, after plowing), 2) after four roller passes (4P), and 3) after ten roller passes (10P), totalling 14 roller passes with previous compaction. The soil was compacted using a water-filled lawn roller with an average mass of 116.7 kg, and a pressure of 956.5 N/m^2 (Fig. 3). EMI and GPR surveys and undisturbed soil sample collections were carried out at each compaction level of NP, 4P and 10P.

2.3. Field data collection

Continuous mode EMI surveys were conducted using a 30 kHz frequency multi-coil EMI sensor (CMD–MINIEXPLORER, GF instruments, Brno, Czech Republic) to collect EC_a data (Fig. 4a). The EMI sensor has three inter-coil spacings (Coil 1: 0.32 m, Coil 2: 0.71 m, and Coil 3: 1.18 m). It can be employed in two coil orientations (vertical coplanar – VCP and horizontal coplanar – HCP), which produces six integral pseudo depths (Short Guide for electromagnetic conductivity mapping and tomography – GF instruments; McNeill, 1980). This study primarily focused on shallow depths (~0.30 m), consistent with both soil sampling and the depth of 500 MHz GPR direct ground wave, the EC_a data from VCP and HCP measurements at the shortest inter-coil spacing (0.32 m) were selected. However, the VCP data from EMI coil 1 showed over 50 % negative values, leading to its exclusion from subsequent analysis. Only the HCP data from coil 1 were retained and henceforth considered as the measured EC_a. Before the survey, the instrument was warmed for a minimum of 30 min to ensure operational stability. Due to the high-temperature stability of the CMD MINIEXPLORER (Short Guide for

[1] Forceful overturning and mashing of the soil underneath topsoil and expose.

Fig. 4. Field data collection using a) electromagnetic induction (EMI) continuous mode, and b) ground-penetrating radar (GPR) common mid-point method (CMP).

electromagnetic conductivity mapping and tomography – GF instruments), no instrumental drift in the EC_a measurements was expected. During the surveys, the instrument was carried using the provided handle with an average height of 0.20 m above the ground, and the same person conducted all the surveys to maintain a consistent instrument height (Fig. 4a).

GPR data were collected using a 500 MHz center frequency GPR system (PulseEKKO Pro, Sensors and Software Inc., Mississauga, Ontario, Canada) (Fig. 4b). A common mid-point (CMP) survey approach was used to obtain the direct ground wave amplitude (A_{DGW}) and direct ground wave velocity (V_{DGW}) at each location. CMP data were collected at four Y locations (1, 3, 5, and 7 m) along each of the X lines spaced at 0.5, 1.5, and 2.5 m intervals (Fig. 2). This method resulted in the collection of three CMP datasets per plot, totalling 12 GPR datasets for each compaction level. The antennas were initially spaced 0.23 m apart (default value), with subsequent antenna movement of 0.1 m step size (transmitter and receiver antennas adjusted by 0.05 m each time). Each CMP dataset comprised seven traces, reaching a final antenna separation of 0.83 m.

Undisturbed soil samples were collected in the same locations with GPR (Fig. 2) for laboratory gravimetric bulk density determination at depth 1 (0.00 – 0.10 m), depth 2 (0.10 – 0.20 m) and depth 3 (0.20 – 0.30 m). Undisturbed soil cores were oven-dried at 105 °C for 24 h, and then they were weighed. The bulk density was determined by dividing the mass of dry soil by the volume of the soil core.

2.4. Pre-processing of geophysical data

Soil EC_a is affected by soil temperature, which is variable; therefore, EMI measured EC_a data were corrected to 25 °C (i.e., EC_{25}) using the soil temperatures measured during the different compaction levels: NP (19.9 °C), 4P (24.7 °C), and 10P (26.3 °C) (Equations (1) and (2) (Sheets and Hendrickx, 1995, U.S. Salinity Laboratory Staff, 1954).

$$EC_{25} = f_T . EC_T \quad (1)$$

$$f_T = 0.4470 + 1.4034e^{\frac{-T}{26.815}} \quad (2)$$

where EC_{25} is the electrical conductivity at 25 °C;
f_T is the temperature conversion factor.
EC_T is the electrical conductivity measured at the temperature T.

Class post maps were prepared with temperature-corrected EC_a data and used to check negative values and filter out outliers. After filtering, interpolated EC_a maps were developed for each compaction level (NP, 4P and 10P) using ordinary (point) kriging with a grid resolution of approximately 0.081 m x 0.081 m after fitting variograms to each dataset. Data points from interpolated EC_a maps were extracted by digitizing at corresponding sampling locations of soil sampling and GPR data collection (as shown in Fig. 2) for subsequent analysis.

In GPR data, the direct ground wave travel times were picked using the GPR processing software's assisted pick processing tool. Picked travel times were plotted with antenna separations to find the V_{DGW} (Annan, 2005). Then, the respective K_r was calculated using the relation: **Equation (3),**

$$K_r = \left(\frac{c}{V_{DGW}}\right)^2 \quad (3)$$

where c is the speed of electromagnetic waves in free space, i.e., 0.3 m/ns (Annan, 2005). SWCs were calculated using **Equation (4),** incorporating calculated K_r (Topp et al., 1980).

$$SWC = -5.3 \times 10^{-2} + 2.92 \times 10^{-2} K_r - 5.5 \times 10^{-4} K_r^2 + 4.3 \times 10^{-6} K_r^3 \quad (4)$$

It is worth noting that the use of Topp's equation may lead to a few percent errors in SWC estimation due to its simplification, particularly given the different compaction levels in this study. However, these errors are generally minor compared to other uncertainties in field conditions and do not significantly impact the overall results of our study, which uses GPR-derived K_r. In addition, GPR traces were plotted, and A_{DGW}s were picked.

Table 2
Descriptive statistics of studied variables.

Variable	Minimum	Maximum	Mean	Standard deviation	Median	Kurtosis	Skewness
SWC_{GPR}	9.24	24.19	17.75	3.67	18.82	−0.11	−0.67
K_r	5.53	12.93	9.52	1.81	10.00	−0.24	−0.50
A_{DGW}	4214	11,953	8880	1549	9097	0.98	−0.74
EC_a	0.08	1.23	0.61	0.36	0.70	−1.35	−0.12
$BD_{(0-30)}$	0.98	1.62	1.31	0.17	1.32	−0.98	−0.10

Sample number, $n = 36$ including 12 from each compaction level; NP, 4P and 10P.

2.5. Data analysis

Descriptive statistics were used to assess the data set. One-way analysis of variance (one-way ANOVA) was conducted on the entire dataset at three compaction levels (NP, 4P and 10P), to assess the significant differences of the applied compaction on the EC_a, K_r, A_{DGW}, SWC estimated from GPR (SWC_{GPR}), and measured soil bulk density. The null hypothesis was that the group means of NP, 4P, and 10P were not equal in the 0.05 significance level. Correlation analyses were carried out between measured average bulk densities of 0–0.30 m depth ($BD_{0\text{-}30}$) with proxies from GPR and EMI. Box plots were created to examine the variability of bulk density, and the percentage changes were calculated to better understand the effect of compaction on the bulk density in each compaction level and depth.

Random forest (RF) is a supervised machine-learning algorithm developed from regression trees. In this study, the RF regression approach was used to select responses from GPR and EMI, facilitating the development of regression models for predicting soil bulk density. RF models were constructed by changing the number of trees and hyperparameters to evaluate the robustness of variable importance rankings, and the most suitable model was selected. The methodology involved a two-step process: 1) a bootstrapped sample of the dataset was used to grow each tree, introducing diversity among the trees; and 2) the importance of each predictor variable was calculated by measuring the decrease in prediction accuracy when the values of that variable were randomly permuted while keeping other variables constant. The variable importance scores were averaged across all trees in each RF model, allowing the ranking of variables based on their relative importance on soil bulk density prediction. This approach provided a comprehensive understanding of which proxies (EC_a or K_r) and variables (A_{DGW}) are most influential in predicting soil bulk density in the studied dataset.

Based on the results of RF, simple linear regression (SLR) and multiple linear regression (MLR) models were developed using the most influential variables to predict soil bulk density. Variance inflation factor (VIF) was estimated to test multicollinearity. Regression models were developed using 24 data points with 8 data points from each compaction level, and model evaluation was conducted with 12 data points, including 4 data points from each compaction level. Data from all three compaction levels were incorporated in both the development and evaluation of the regression models to increase the variability of bulk density. The data for developing and evaluating the regression models were randomly selected in the NP; then, the exact locations were used for the 4P and 10P. Developed regression models were applied to the evaluation dataset. The accuracy of the developed regression models was evaluated by comparing the predicted and measured bulk densities. This comparison was conducted using a 1:1 line, the Root Mean Square Error (RMSE), and a two-tailed *t*-test.

3. Results and discussion

3.1. Variability of data and analysis of variance

Descriptive statistics of the dataset is shown in Table 2. When considering the sensor data, the range of SWC and K_r was comparatively higher than the range of EC_a in the studied dataset. All the datasets were normally distributed (i.e., Kurtosis < 4 and Skewness < 2).

Table 3
Results of one-way analysis of variance (ANOVA) and Tukey tests of no passes (NP), after four passes (4P) and after ten passes (10P) at the 0.05 significance level.

Variable	n	Mean – NP	Mean – 4P	Mean – 10P	F-value	*p*-value
$BD_{0\text{-}30}$ (g/cm^3)	36	1.11^a	1.33^b	1.48^c	53.15	0.000
K_r	36	7.739^a	9.952^b	10.879^b	19.93	0.000
SWC_{GPR}	36	14.111^a	18.688^b	20.466^b	19.97	0.000
A_{DGW} (mV)	36	7687^a	9018^b	9936^b	9.49	0.001
EC_a (mS/m)	36	0.1689^a	0.7021^b	0.9481^c	82.45	0.000

n – number of samples; *p*-value – probability value; different letters$^{(a, b, c)}$ within the same row indicate a significant difference between different compaction efforts (NP, 4P and 10P).
The mean difference is significant at the 0.05 level: $F_{crit.} = 3.28$.

According to the one-way ANOVA results, the probability values (*p-value*) of all the variables were less than the 0.05 significance level. Therefore, the null hypothesis was rejected, indicating that not all means are equal (Table 3). F-values explained the variation between the group and within the group whereby the F-value is higher than the $F_{critical}$ value (3.28) in the datasets. Therefore, the mean difference is significant in the dataset under the 0.05 significance level. With the influence of applied soil compaction, mean values increased across all datasets (Table 3), showing the influence of soil compaction on GPR and EMI responses (**Appendix 1**). The Tukey test results imply significant differences in bulk density and EC_a from EMI between NP, 4P and 10P. However, there is no significant difference between 4P and 10P in GPR responses (K_r, A_{DGW}, and SWC_{GPR}). Nevertheless, there is a significant difference between the pre-compaction (NP) and post-compaction (4P and 10P) levels. According to the one-way ANOVA results, all the variables responded to the applied roller compaction.

3.2. Variability of bulk density with applied compaction

The box plot shows the variability of measured $BD_{0\text{-}30}$ under three compaction levels (Fig. 5a). As expected, NP marked the lowest bulk density, and bulk density gradually increased from NP to 4P and then from 4P to 10P with the applied roller compaction (Fig. 5a). On the other hand, the $BD_{0\text{-}30}$variation decreases with applied roller compaction (Fig. 5a) as the depth 1 (upper depths) has lower bulk densities compared to depth 3 in NP. With the applied compaction, upper depths are compacted easily. Therefore, depth-based variability was minimal in 10P compared to the NP (Fig. 5b).

Bulk density increased across all three tested soil depths, from NP to 4P and from 4P to 10P. Depth 1 showed the highest percentage increase, with 25.5 % from NP to 4P and 16.9 % from 4P to 10P, as expected, compared to depths 2 and 3 (Fig. 5c). The roller compaction affects all depths due to applied pressure, however, the relative effect of compaction diminishes with the depth. Furthermore, the percentage change is greater from NP to 4P in depths 1 and 2 than from 4P to 10P. This is because the soil in the NP was loosely packed, making it easier to compact compared to the soil after the 4P, which had already undergone compaction with four roller passes (Fig. 5c). The percentage increase in depth 3 remained consistent, with 7.8

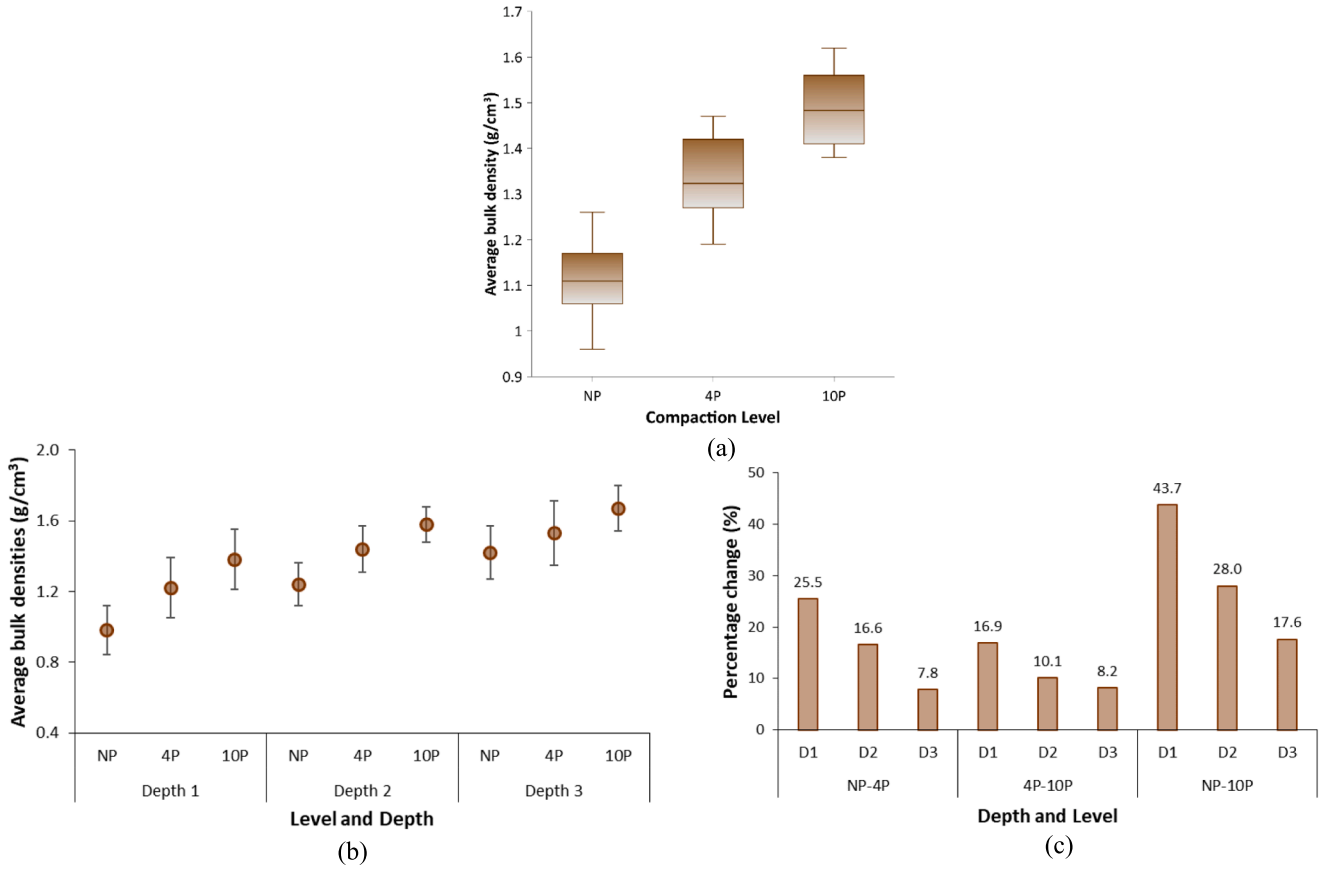

Fig. 5. (a) Boxplot of average bulk densities (0 – 0.30 m) measured under three soil compaction levels; NP – no passes, 4P – four roller passes, and 10P – ten roller passes, (b) variability of bulk densities in three depths (0 – 0.10 m; 0.10 – 0.20 m; 0.20 – 0.30 m) and three compaction levels (NP, 4P, and 10P; Each data point shows the mean value and standard deviation (n = 12)), and (c) Percentage change of soil bulk density in three depths, from NP to 4P, 4P to 10P, and NP to 10P (totalling 14 roller passes).

% from NP to 4P and 8.2 % from 4P to 10P.

3.3. Correlation analysis

All the correlations between the $BD_{0\text{-}30}$ and K_r, A_{DGW} (from GPR) and EC_a (from EMI) are significant at a 95 % ($\alpha = 0.05$) probability level. The relationship between the $BD_{0\text{-}30}$ and proxies from EMI and GPR showed strong positive correlations. The Pearson correlation coefficient (r) between the $BD_{0\text{-}30}$ and K_r, as well as A_{DGW} from GPR, showed values of r = 0.72 (p = 0.000) and r = 0.71 (p = 0.000), respectively (Fig. 6a and b). On the other hand, r = 0.89 (p = 0.000) between the average bulk density and EC_a measured from EMI (Fig. 6c).

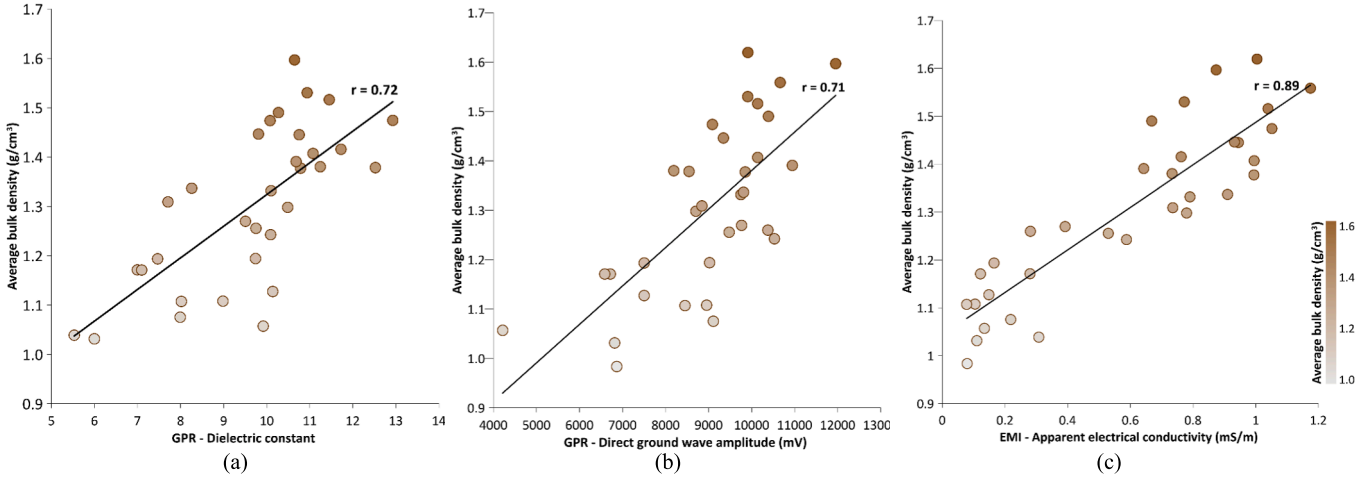

Fig. 6. Correlation between average bulk density (0 – 0.30 cm) and a) dielectric constant (K_r) estimated from ground-penetrating radar (GPR), b) direct ground wave amplitude of GPR (A_{DGW}), and c) apparent electrical conductivity (EC_a) measured from electromagnetic induction horizontal dipole orientation.

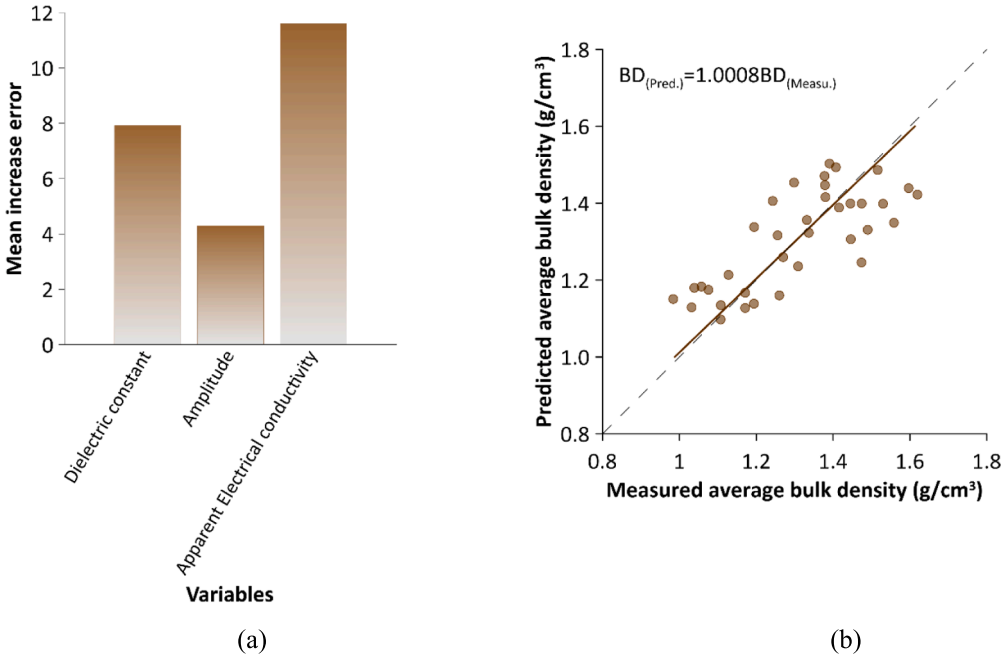

Fig. 7. Regression random forest (RF) results: a) variable importance, and b) scatter plots of measured vs predicted bulk densities with the RF model. The dashed line corresponds to the 1:1 line and the solid line corresponds to the linear fit.

Table 4
Regression equations, coefficient of determination (R^2), root mean square error (RMSE), *p*-value and variance inflation factor (VIF) of developed regression models.

Regression Equation	R^2	RMSE (g/cm^3)	*p*-value	VIF
$BD_{0\text{-}30} = 1.043 + 0.418\ EC_a$	80	0.075	0.000	
$BD_{0\text{-}30} = 0.7840 + 0.05612\ K_r$	63	0.090	0.000	
$BD_{0\text{-}30} = 0.93 + 0.0212\ K_r + 0.2734\ EC_a$	83	0.062	0.000	K_r – 2.606 EC_a – 2.606

3.4. Random forest

By considering both linear and non-linear behaviors, the RF regression provided valuable insights into the factors influencing the prediction of soil bulk density. Among the different variables considered, EC_a measured using EMI emerged as the primary contributor to the prediction of soil bulk density since EC_a showed the highest mean increase error compared to K_r and A_{DGW} (Fig. 7a). Furthermore, in the RF regression, the variable importance of K_r was found to be higher than that of A_{DGW} (Fig. 7a). In the cross-validation process used to assess the reliability of the developed RF model, the comparison between measured and model-predicted bulk densities along the 1:1 line illustrated the effectiveness of the model in predicting soil bulk density with the included parameters (Fig. 7b). The RMSE of the prediction was found to be 0.11 g/cm^3.

3.5. Development of linear regression models

Based on the variable importance of RF regression for predicting soil bulk density, EC_a and K_r data were selected to develop the SLR and then MLR models (Table 4). The SLR model developed with EC_a showed a higher R^2 than that was developed with K_r (Table 4). The VIF of the MLR is < 5 for both K_r and EC_a, indicating the absence of multicollinearity of

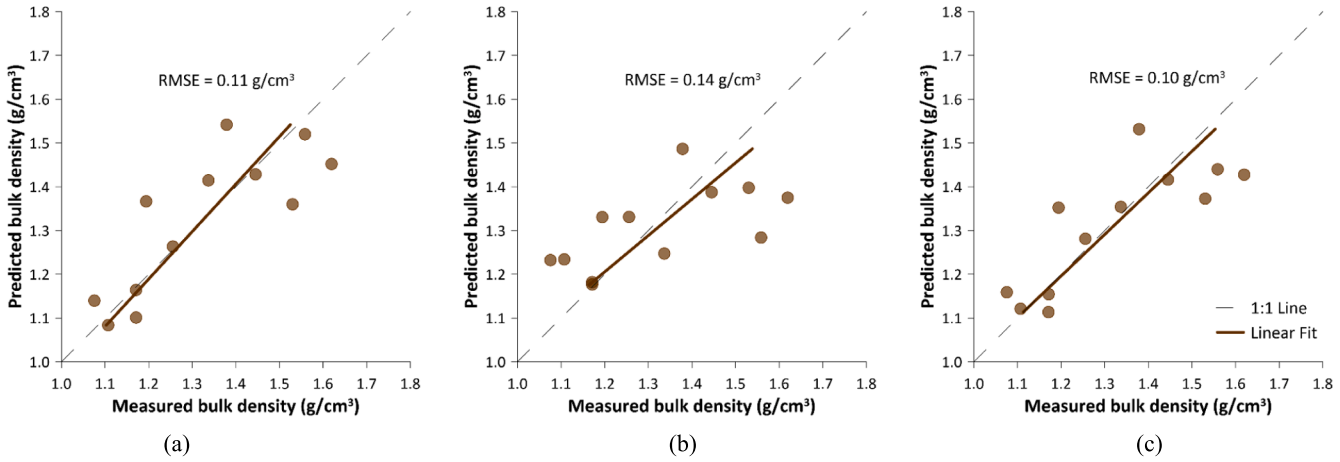

Fig. 8. Scatter plots of measured soil bulk density and simple linear regression (SLR) and multiple linear regression (MLR) model predicted soil bulk density. SLR model predicted; a) apparent electrical conductivity (EC_a), and b) dielectric constant (K_r) and c) MLR model predicted. The dash lines correspond to the 1:1 line.

Table 5
Summary of statistical comparison of measured and predicted bulk densities of regression models (at 0.05 significance level; degree of freedom = 11; t_{table} = 2.201).

Regression	$t_{calculated}$	Slope = 1	Deviation from 1:1 line
$BD_{0\text{-}30}$- EC_a	0.084	NS	No
$BD_{0\text{-}30}$-K_r	0.703	NS	No
$BD_{0\text{-}30}$- K_r and EC_a	0.583	NS	No

$BD_{0\text{-}30}$ – average bulk density, EC_a – Apparent electrical conductivity measured from electromagnetic induction (EMI), K_r – dielectric constant estimated from ground-penetrating radar (GPR), NS – Nonsignificant.

dependent variables. Additionally, the MLR model demonstrated a higher R^2 and lower RMSE compared to the developed SLR models (Table 4).

3.6. Evaluation of linear regression models

The evaluation of the developed linear regression models revealed that the prediction accuracy of these models is satisfactory, with most data points plotted closer to or scattered around the 1:1 line (Fig. 8). The comparison between the predicted bulk density from regression models and the measured bulk density from soil samples showed no significant from the 1:1 line at 0.05 significance level (the regression slope between predicted and measured bulk density = 1) (Table 5). These results reveal that the three regression models could predict soil bulk density accurately. Among the SLR models, by comparing with measured bulk density, EC_a predicted bulk density showed the lowest RMSE value of 0.11 g/cm^3, while it was 0.14 g/cm^3 for K_r predicted bulk density. On the other hand, MLR models showed the lowest RMSE value of 0.10 g/cm^3 compared to the two SLR models. All three regression models underestimated the predicted bulk densities for measured values exceeding 1.5 g/cm^3 (Fig. 8). The RMSE observed in this study (<0.14 g/cm^3) is within the RMSEs observed in the other bulk density predictions, such as pedotransfer functions under various land use conditions (Sevastas et al., 2018; Palladino et al., 2021).

When considering a 30 cm soil profile as a three-phase system (i.e., consisting of solid, water and air), the quantities of solid and water content remain constant, while air content reduces during compaction with applied roller passes. Consequently, the air-filled pore space decreases during compaction, leading to an increase in saturation percentage due to the reduction in porosity with increasing bulk density. In this study, the air content was reduced by 7.5 cm (from 13.2 to 5.7 cm) from NP to 10P (**Calculation – Appendix 2**). After the roller passes, mineral particles become densely packed, reducing macropores while the amount of water remains constant. This results in an increased amount of water and clay content per unit volume compared to the NP, thereby increasing bulk K_r and EC_a, which facilitates electrical conductivity pathways.

This study introduces a novel approach by aiming to predict soil bulk density using GPR and EMI responses, rather than focusing on how soil compaction affects GPR and EMI responses. As the initial step, certain limitations were identified in this study. The research was conducted on a specific soil type, namely Loamy sand-podzolic soil, characterized by relatively higher percentages of sand and gravel content compared to typical agricultural soils. GPR and EMI responses are primarily influenced by SWC and soil salinity, and broadly, EC_a measurements rely on several soil properties, including bulk density/porosity, soil texture/mineralogy, and soil organic matter. However, at the studied site and during the experiment, the variability of EC_a and SWC values was observed to be relatively low with a narrow range. Due to the low values and limited range of SWC under this study, the impact of SWC on the soil compaction and, thus, on bulk density may have been minimal. With low variability in EC_a and SWC, EC_a values likely responded strongly to applied soil compaction. In high salinity or SWC environments, EMI responses predominantly indicate soil salinity or SWC states, with minimal influence from bulk density.

In both calibration and evaluation datasets, our study observed relatively low values and variability in the EC_a values measured by EMI. It is noteworthy that, not only in our present study but also in previous research conducted at the same site with multi-coil and multi-frequency EMI instruments, consistently low EC_a values and limited variability were observed (Altdorff et al., 2018, 2020; Badewa et al., 2018, 2019; Pathirana et al., 2024). Given this established context, the controlled conditions of our study, which are more likely to be a laboratory experiment on boreal podzolic soil, may limit the broader applicability of our findings. Despite facing the primary limitation of low EC_a values and their limited range, our study lays the foundation for more comprehensive investigation in the future. As an initial step, the present study analyzed the measured EC_a data, while subsequent research should expand on the proposed approach by incorporating advanced data processing techniques, including calibration, conversion, and inversion of EC_a data (von Hebel et al., 2019) to enhance the applicability of our novel approach in diverse soil environments.

Moreover, soil compaction varies across different soil textures, SWCs, and organic matter contents, limiting the responses and applicability of GPR and EMI techniques in different textures (Hamza and Anderson, 2005). For future research directions, it is imperative to establish and refine prediction models under diverse conditions to evaluate their applicability across varying scenarios. Therefore, the same approach, along with integrating petrophysical relationships involving EC_a, bulk density/porosity, SWC/saturation and pore water electrical conductivity across various soil textures, is essential. This comprehensive approach is necessary to advance this novel method and enhance its effectiveness in predicting soil bulk density non-destructively, serving as a valuable soil compaction assessment tool over the agricultural landscape.

4. Conclusion

In this study, apparent electrical conductivity (EC_a) from electromagnetic induction (EMI), along with the dielectric constant (K_r) and direct ground wave amplitude (A_{DGW}) from ground-penetrating radar (GPR), were employed to predict soil bulk density, a key indicator of soil compaction. The proxies from GPR (K_r and A_{DGW}) and EMI (EC_a) responded effectively to applied soil compaction, showing strong positive correlations with measured $BD_{0\text{-}30}$. Random forest regression models identified EC_a as the most important variable for predicting soil bulk density, outperforming both K_r and A_{DGW} from GPR, leading to more accurate bulk density predictions at the studied site. Additionally, simple and multiple linear regression models developed for bulk density predictions using two proxies achieved higher R^2 values (>0.50). Consequently, GPR and EMI have emerged as promising non-destructive technologies, offering the advantage of assessing larger sample volumes. While traditional point-scale measurements remain essential for calibrating predictive models, these techniques show significant potential for extending soil bulk density estimation across larger agricultural landscapes.

This study demonstrated that both EC_a from EMI and K_r from GPR can effectively predict soil bulk density, showing strong correlations with measured values. While EMI using SLR proved sufficient for soil bulk density assessments at the studied site, the integration of GPR data, particularly through MLR models, offered slight improvements in prediction accuracy by incorporating SWC, which plays a significant role in influencing EC_a. The combined use of EMI and GPR provides a more robust, non-destructive approach for bulk density estimation, with GPR contributing valuable data on SWC. Further research is needed to refine prediction models under diverse conditions to improve their applicability. Given that both EC_a and GPR measurements are influenced by various soil properties and conditions, response variations across different soils and management practices may occur. Additionally, differences in soil compaction across textures may affect the effectiveness of employing these geophysical techniques. Exploring these factors will be crucial for optimizing the integrated use of EMI and GPR to predict soil bulk density in field applications.

Funding

This research was funded by Natural Sciences and Engineering Research Council of Canada, Discovery Grant (NSERC-DG): RGPIN-2019–04614, Industry, Energy and Innovation (IET) of the Government of Newfoundland and Labrador, Grant: 5404–1962-102, and Grenfell Campus, Memorial University of Newfoundland.

CRediT authorship contribution statement

Sashini Pathirana: Writing – original draft, Visualization, Methodology, Investigation, Formal analysis, Data curation, Conceptualization. **Sébastien Lambot:** Writing – review & editing, Validation, Supervision, Methodology. **Manokararajah Krishnapillai:** Writing – review & editing, Validation. **Mumtaz Cheema:** Writing – review & editing, Visualization. **Christina Smeaton:** Writing – review & editing, Validation, Supervision. **Lakshman Galagedara:** Writing – review & editing, Validation, Supervision, Resources, Project administration, Methodology, Investigation, Funding acquisition, Conceptualization.

Declaration of competing interest

The authors declare that they have no known competing financial interests or personal relationships that could have appeared to influence the work reported in this paper.

Data availability

Data will be made available on request.

Acknowledgement

The authors would like to express sincere gratitude to Jayamini Rathnayake, Clinton Mensah, Annabel Arnott, Salman Afzal, Golam Rabbani, Juwonlo Dahunsi, and Lanthika Dnapala for their assistance in field data collection.

The authors extend special appreciation to Adrian Reid and the other staff members of the Department of Fisheries, Forestry, and Agriculture, Government of Newfoundland and Labrador, for their provision and oversight of the research field.

Appendix 1

(See Fig. A1.).

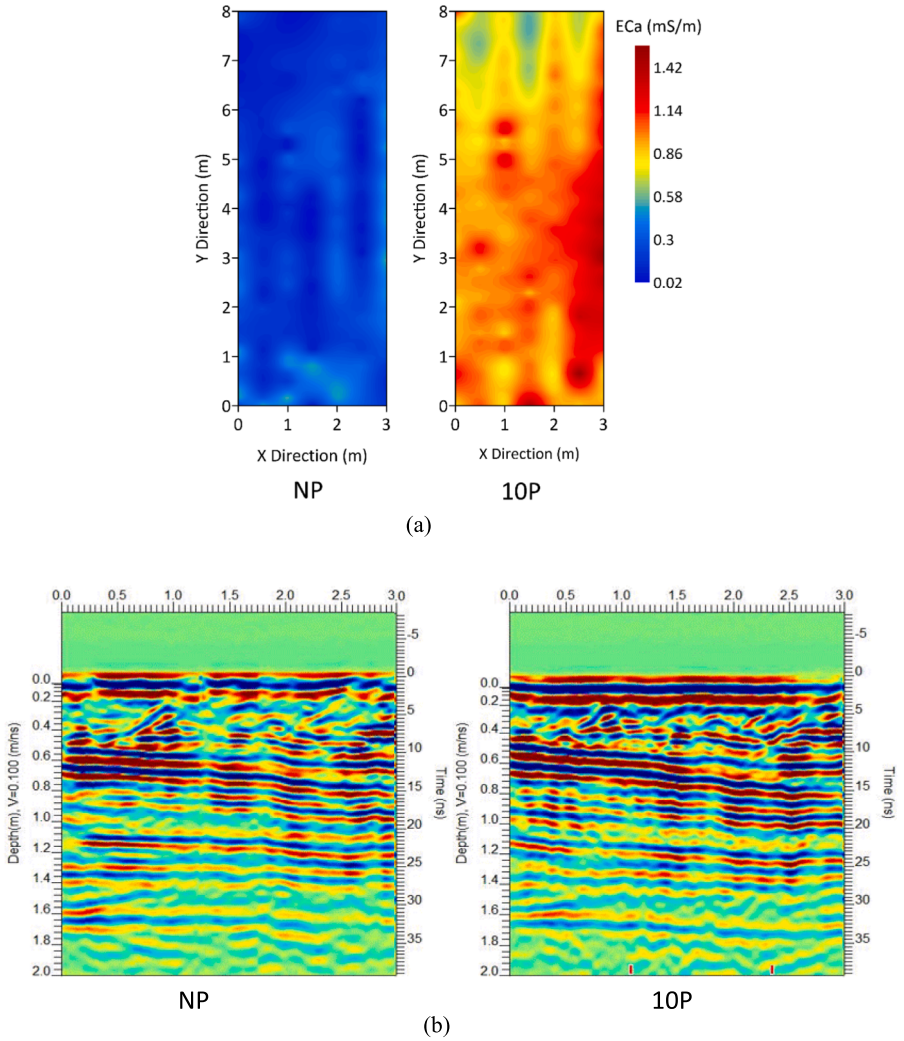

Fig. A1. Compaction effect on a) apparent electrical conductivity measured from electromagnetic induction (EMI) and b) radargram from ground-penetrating radar (GPR), under no passes (NP) and after 10 roller passes (10P).

Appendix 2

Calculation

Bulk density = mass / bulk volume.

When consider 30 cm depth of a similar area (A),

NP→1.11 gcm^{-3} = (mass (g)/A (cm^2))*1/30 (cm)

mass/A = 1.11 * 30

Soil depth after 10P – x cm.

10P→1.48 gcm^{-3}= (mass/A)*1/x

x = (1.11 * 30)/1.48 = **22.5 cm**.

After 10P, 30 cm depth reduced to 22.5 cm.

Water amount as a depth, in NP (30 cm depth) = 14.1/100 * 30 cm = **4.23 cm**.

Soil water content after 10P (22.5 cm depth) = 4.23 cm/22.5 cm * 100 = **18.8 %**.

After 10P soil water content increases.

Porosity = 1 – Bulk density/Particle density.

Particle density assumed as 2.66 gcm^{-3}.

Porosity in NP = (1–(1.11 gcm^{-3}/2.66 gcm^{-3})) = 0.58.

Void content = 0.58, and Solid content = 0.42.

Solid content in 30 cm depth = 42/100 * 30 cm = **12.6 cm**.

Solid content = 12.6 Water content = 4.23 Air content = 13.2 → NP.

Solid content = 12.6 Water content = 4.23 Air content = 5.7 → 10P.

All calculations are based on measured $BD_{0\text{-}30}$ and GPR measured SWC showing in Table 3.

References

Akinsunmade, A., 2021. GPR imaging of traffic compaction effects on soil structures. Acta Geophysica 69 (2), 643–653. https://doi.org/10.1007/s11600-020-00530-0.

Akinsunmade, A., Tomecka-Suchoń, S., Pysz, P., 2019. Correlation between agrotechnical properties of selected soil types and corresponding GPR response. Acta Geophysica 67 (6), 1913–1919. https://doi.org/10.1007/s11600-019-00349-4.

Akinsunmade, A., Tomecka-Suchoń, S., Kiełbasa, P., Juliszewski, T., Pysz, P., Karczewski, J., Zagórda, M., 2021. GPR geophysical method as a remediation tool to determine zones of high penetration resistance of soil. Journal of Physics: Conference Series 1782 (1), 012001. https://doi.org/10.1088/1742-6596/1782/1/012001.

Akramkhanov, A., Brus, D.J., Walvoort, D.J.J., 2014. Geostatistical monitoring of soil salinity in Uzbekistan by repeated EMI surveys. Geoderma 213, 600–607. https://doi.org/10.1016/j.geoderma.2013.07.033.

Al-Gaadi, K.A., 2012. Employing electromagnetic induction technique for the assessment of soil compaction. American Journal of Agricultural and Biological Sciences 7 (4), 425–434. https://doi.org/10.3844/ajabssp.2012.425.434.

Alsharahi, G., Driouach, A., Faize, A., 2016. Performance of GPR influenced by electrical conductivity and dielectric constant. Procedia Technology 22, 570–575. https://doi.org/10.1016/j.protcy.2016.01.118.

Altdorff, D., Galagedara, L., Nadeem, M., Cheema, M., Unc, A., 2018. Effect of agronomic treatments on the accuracy of soil moisture mapping by electromagnetic induction. Catena 164, 96–106. https://doi.org/10.1016/j.catena.2017.12.036.

Altdorff, D., Sadatcharam, K., Unc, A., Krishnapillai, M., Galagedara, L., 2020. Comparison of multi-frequency and multi-coil electromagnetic induction (EMI) for mapping properties in shallow podsolic soils. Sensors 20 (8). https://doi.org/10.3390/s20082330. Article 8.

Annan, A.P., 2005. Ground-Penetrating Radar. In: Butler, D.K. (Ed.), Near-Surface Geophysics, Vol. 13. Society of Exploration Geophysicists. https://doi.org/10.1190/1.9781560801719.ch11.

Archie, G.E., 1942. The electrical resistivity log as an aid in determining some reservoir characteristics. Transactions of the AIME 146 (01), 54–62. https://doi.org/10.2118/942054-G.

Badewa, E., Unc, A., Cheema, M., Kavanagh, V., Galagedara, L., 2018. Soil moisture mapping using multi-frequency and multi-coil electromagnetic induction sensors on managed podzols. Agronomy 8 (10), 224. https://doi.org/10.3390/agronomy8100224.

Badewa, E., Unc, A., Cheema, M., Galagedara, L., 2019. Temporal stability of soil apparent electrical conductivity (ECa) in managed podzols. Acta Geophysica 67 (4), 1107–1118. https://doi.org/10.1007/s11600-019-00306-1.

Batey, T., 2009. Soil compaction and soil management – a review. Soil Use and Management 25 (4), 335–345. https://doi.org/10.1111/j.1475-2743.2009.00236.x.

Batey, T., McKenzie, D.C., 2006. Soil compaction: Identification directly in the field. Soil Use and Management 22 (2), 123–131. https://doi.org/10.1111/j.1475-2743.2006.00017.x.

Birchak, J.R., Gardner, C.G., Hipp, J.E., Victor, J.M., 1974. High dielectric constant microwave probes for sensing soil moisture. Proceedings of the IEEE 62 (1), 93–98. https://doi.org/10.1109/PROC.1974.9388.

Brevik, E.C., Fenton, T.E., 2002. Influence of soil water content, clay, temperature, and carbonate minerals on electrical conductivity readings taken with an EM-38. Soil Survey Horizons 43, 9–13.

Corwin, D.L., Lesch, S.M., 2014. A simplified regional-scale electromagnetic induction—Salinity calibration model using ANOCOVA modeling techniques. Geoderma 230–231, 288–295. https://doi.org/10.1016/j.geoderma.2014.03.019.

De Carlo, L., Vivaldi, G.A., Caputo, M.C., 2022. Electromagnetic induction measurements for investigating soil salinization caused by saline reclaimed water. Atmosphere 13 (1), 73-. https://doi.org/10.3390/atmos13010073.

De Moraes, M.T., Debiasi, H., Carlesso, R., Franchini, J.C., Da Silva, V.R., Da Luz, F.B., 2017. Age-hardening phenomena in an oxisol from the subtropical region of Brazil. Soil and Tillage Research 170, 27–37. https://doi.org/10.1016/j.still.2017.03.002.

De Moraes, M.T., Debiasi, H., Franchini, J.C., Bonetti, J.D.A., Levien, R., Schnepf, A., Leitner, D., 2019. Mechanical and hydric stress effects on maize root system development at different soil compaction levels. Frontiers in Plant Science 10, 1358. https://doi.org/10.3389/fpls.2019.01358.

Doolittle, J.A., Brevik, E.C., 2014. The use of electromagnetic induction techniques in soils studies. Geoderma 223–225, 33–45. https://doi.org/10.1016/j.geoderma.2014.01.027.

Doolittle, J., Petersen, M., Wheeler, T., 2001. Comparison of two electromagnetic induction tools in salinity appraisals. Journal of Soil and Water Conservation 56 (3), 257–262.

Ferrara, C., Di Tullio, V., Barone, P.M., Mattei, E., Lauro, S.E., Proietti, N., Capitani, D., Pettinelli, E., 2013. Comparison of GPR and unilateral NMR for water content measurements in a laboratory scale experiment. Near Surface Geophysics 11 (2), 143–153. https://doi.org/10.3997/1873-0604.2012051.

Freeland, R.S., Yoder, R.E., Ammons, J.T., 1998. Mapping shallow underground features that influence site-specific agricultural production. Journal of Applied Geophysics 40 (1–3), 19–27. https://doi.org/10.1016/S0926-9851(98)00014-7.

Galagedara, L.W., Parkin, G.W., Redman, J.D., 2003a. An analysis of the ground-penetrating radar direct ground wave method for soil water content measurement. Hydrological Processes 17 (18), 3615–3628. https://doi.org/10.1002/hyp.1351.

Galagedara, L.W., Parkin, G.W., Redman, J.D., Endres, A.L., 2003b. Assessment of soil moisture content measured by borehole GPR and TDR under transient irrigation and drainage. Journal of Environmental and Engineering Geophysics 8 (2), 77–86. https://doi.org/10.4133/JEEG8.2.77.

Galambošová, J., Macák, M., Rataj, V., Barát, M., Misiewicz, P.A., 2020. Determining trafficked areas using soil electrical conductivity–a pilot study. Acta Technol. Agric. 23, 1–6. https://doi.org/10.2478/ata-2020-0001.

Gates, Z.W., Galagedara, L.W., Ziegler, S.E., 2023. Combining ground penetrating radar methodologies enables large-scale mapping of soil horizon thickness and bulk density in boreal forests. Soil Use and Management 39 (4), 1289–1303. https://doi.org/10.1111/sum.12964.

Hamza, M.A., Anderson, W.K., 2005. Soil compaction in cropping systems: A review of the nature, causes and possible solutions. Soil & Tillage Research 82 (2), 121–145. https://doi.org/10.1016/j.still.2004.08.009.

Hanxiao, X., Yingui, C., Gubai, L., Shufei, W., Jinman, W., Zhongke, B., 2022. Variability in reconstructed soil bulk density of a high moisture content soil: A study on feature identification and ground penetrating radar detection. Environmental Earth Sciences 81 (9), 249. https://doi.org/10.1007/s12665-022-10365-1.

Hoefer, G., Bachmann, J., & Hartge, K. H., 2010. Can the EM38 probe detect spatial patterns of subsoil compaction? In proximal soil sensing (pp. 265–273). Springer Netherlands. https://doi.org/10.1007/978-90-481-8859-8_22.

Huisman, J.A., Hubbard, S.S., Redman, J.D., Annan, A.P., 2003. Measuring soil water content with ground penetrating radar: a review. Vadose Zone Journal 2 (4), 476–491. https://doi.org/10.2113/2.4.476.

Jonard, F., Mahmoudzadeh, M., Roisin, C., Weihermüller, L., André, F., Minet, J., Vereecken, H., Lambot, S., 2013. Characterization of tillage effects on the spatial variation of soil properties using ground-penetrating radar and electromagnetic induction. Geoderma 207–208, 310–322. https://doi.org/10.1016/j.geoderma.2013.05.024.

Kar, S.K., Patra, S., Singh, R.M., Sankar, M., Kumar, S., Singh, D., Madhu, M., Singla, S., 2023. Impact of land use reformation on soil hydraulic properties and recovery potential of conservation tillage in India's North-West Himalayan region. Ecohydrology & Hydrobiology 23 (2), 290–303. https://doi.org/10.1016/j.ecohyd.2022.12.008.

Klotzsche, A., Jonard, F., Looms, M.C., van der Kruk, J., Huisman, J.A., 2018. Measuring soil water content with ground penetrating radar: A decade of progress. Vadose Zone Journal 17 (1), 180052. https://doi.org/10.2136/vzj2018.03.0052.

Krzic, M., Page, H., Newman, R., & Broersma, K., 2005. Aspen regeneration, forage production, and soil compaction on harvested and grazed boreal aspen stands. Journal of Ecosystems and Management. https://doi.org/10.22230/jem.2005v5n2a296.

Lambot, S., Slob, E.C., van den Bosch, I., Stockbroeckx, B., Vanclooster, M., 2004. Modeling of ground-penetrating radar for accurate characterization of subsurface electric properties. IEEE Transactions on Geoscience and Remote Sensing 42 (11), 2555–2568.

Lambot, S., Weihermüller, L., Huisman, J.A., Vereecken, H., Vanclooster, M., Slob, E.C., 2006. Analysis of air-launched ground-penetrating radar techniques to measure the soil surface water content. Water Resources Research 42, W11403. https://doi:11410.11029/12006WR005097.

Lardy, J.M., DeSutter, T.M., Daigh, A.L.M., Meehan, M.A., Staricka, J.A., 2022. Effects of soil bulk density and water content on penetration resistance. Agricultural & Environmental Letters 7 (2), e20096.

Liu, H., Colombi, T., Jäck, O., Keller, T., Weih, M., 2022. Effects of soil compaction on grain yield of wheat depend on weather conditions. Science of the Total Environment 807, 150763. https://doi.org/10.1016/j.scitotenv.2021.150763.

McNeill, J.D., 1980. Electromagnetic Terrain Conductivity Measurement at Low Induction Numbers; Technical Note TN-6. Geonics Ltd., Mississauga, ON, Canada.

Meng, C., Yang, W., Wang, D., Hao, Z., Li, M., 2023. Development and testing of vehicle-mounted soil bulk density detection system. Measurement 211, 112604. https://doi.org/10.1016/j.measurement.2023.112604.

Mensah, C., Katanda, Y., Krishnapillai, M., Cheema, M., Galagedara, L., 2023. Estimation of soil water content using electromagnetic induction sensors under different land uses. Environmental Research Communications 5 (8), 085002. https://doi.org/10.1088/2515-7620/acebbd.

Milne, R.M., Haynes, R.J., 2004. Comparative effects of annual and permanent dairy pastures on soil physical properties in the Tsitsikamma region of South Africa. Soil Use and Management 20 (1), 81–88. https://doi.org/10.1111/j.1475-2743.2004.tb00340.x.

Minet, J., Lambot, S., Slob, E.C., Vanclooster, M., 2010. Soil surface water content estimation by full-waveform GPR signal inversion in the presence of thin layers. IEEE Transactions on Geoscience and Remote Sensing 48 (3), 1138–1150. https://doi.org/10.1109/TGRS.2009.2031907.

Nawaz, M.F., Bourrié, G., Trolard, F., 2013. Soil compaction impact and modelling. A Review. Agronomy for Sustainable Development 33 (2), 291–309. https://doi.org/10.1007/s13593-011-0071-8.

Palladino, M., Romano, N., Pasolli, E., & Nasta, P., 2022. Developing pedotransfer functions for predicting soil bulk density in Campania. Geoderma, 412, 115726-. https://doi.org/10.1016/j.geoderma.2022.115726.

Pathirana, S., Lambot, S., Krishnapillai, M., Cheema, M., Smeaton, C., & Galagedara, L., 2023. Ground-penetrating radar and electromagnetic induction: Challenges and opportunities in agriculture. Remote Sensing, 15(11), Article 11. https://doi.org/10.3390/rs15112932.

Pathirana, S., Lambot, S., Krishnapillai, M., Smeaton, C., Cheema, M., Galagedara, L., 2024. Potential of ground-penetrating radar to calibrate electromagnetic induction for shallow soil water content estimation. Journal of Hydrology, Volume 633, 130957, ISSN 0022-1694, https://doi.org/10.1016/j.jhydrol.2024.130957.

Ren, L., D'Hose, T., Borra-Serrano, I., Lootens, P., Hanssens, D., De Smedt, P., Cornelis, W.M., Ruysschaert, G., 2022. Detecting spatial variability of soil compaction using soil apparent electrical conductivity and maize traits. Soil Use and Management 38 (4), 1749–1760. https://doi.org/10.1111/sum.12812.

Romero-Ruiz, A., O'Leary, D., Daly, E., Tuohy, P., Milne, A., Coleman, K., & Whitmore, A. P. (2024). An agrogeophysical modelling framework for the detection of soil compaction spatial variability due to grazing using field-scale electromagnetic induction data. Soil Use and Management, 40(2). https://doi.org/10.1111/sum.13039.

Romero-Ruiz, A., Linde, N., Keller, T., Or, D., 2018. A review of geophysical methods for soil structure characterization. Reviews of Geophysics 56 (4), 672–697. https://doi.org/10.1029/2018RG000611.

Roodposhti, H.R., Hafizi, M.K., Kermani, M.R.S., 2020. Ground penetrating radar for water content and compaction evaluation: A laboratory test on construction material. Journal of Environmental and Engineering Geophysics 25 (2), 169–179. https://doi.org/10.2113/JEEG19-035.

Schmäck, J., Weihermüller, L., Klotzsche, A., Von Hebel, C., Pätzold, S., Welp, G., Vereecken, H., 2022. Large-scale detection and quantification of harmful soil compaction in a post-mining landscape using multi-configuration electromagnetic induction. Soil Use and Management 38 (1), 212–228. https://doi.org/10.1111/sum.12763.

Sevastas, S., Gasparatos, D., Botsis, D., Siarkos, I., Diamantaras, K. I., & Bilas, G., 2018. Predicting bulk density using pedotransfer functions for soils in the Upper Anthemountas basin, Greece. Geoderma Regional, 14, e00169-. https://doi.org/10.1016/j.GEODRS.2018.e00169.

Topp, G.C., Davis, J.L., Annan, A.P., 1980. Electromagnetic determination of soil water content: Measurements in coaxial transmission lines. Water Resources Research. 16, 574–582.

von Hebel, C., van der Kruk, J., Huisman, J. A., Mester, A., Altdorff, D., Endres, A. L., Zimmermann, E., Garré, S., & Vereecken, H. (2019). Calibration, Conversion, and Quantitative Multi-Layer Inversion of Multi-Coil Rigid-Boom Electromagnetic Induction Data. Sensors, 19(21), 4753-. https://doi.org/10.3390/s19214753.

Wang, P., Hu, Z., Zhao, Y., Li, X., 2016. Experimental study of soil compaction effects on GPR signals. Journal of Applied Geophysics 126, 128–137. https://doi.org/10.1016/j.jappgeo.2016.01.019.

Wijewardana, Y.N.S., Shilpadi, A.T., Mowjood, M.I.M., Kawamoto, K., Galagedara, L.W., 2017. Ground-penetrating radar (GPR) responses for sub-surface salt contamination and solid waste: Modeling and controlled lysimeter studies. Environmental Monitoring and Assessment 189 (2), 57. https://doi.org/10.1007/s10661-017-5770-4.

Wu, K., & Lambot, S., 2022. Analysis of low-frequency drone-borne GPR for root-zone soil electrical conductivity characterization. IEEE Transactions on Geoscience and Remote Sensing, vol. 60, pp. 1-13, 2022, Art no. 2006213, doi: 10.1109/TGRS.2022.3198431.

Wu, K., Rodriguez, G.A., Zajc, M., Jacquemin, E., Clément, M., De Coster, A., Lambot, S., 2019. A new drone-borne GPR for soil moisture mapping. Remote Sensing of Environment 235, 111456.